*Journal of Sound and Vibration* (2001) **246**(3), 505–524
doi:10.1006/jsvi.2001.3670, available online at http://www.idealibrary.com on IDEAL®

# DEVELOPMENT AND VALIDATION OF A NEW EXPERIMENTAL METHOD TO IDENTIFY DAMPING MATRICES OF A DYNAMIC SYSTEM

J.-H. Lee and J. Kim

*Structural Dynamics Research Laboratory, Mechanical Engineering Department, University of Cincinnati, Cincinnati, OH* 45221-0072, *U.S.A. E-mail: jay.kim@uc.edu*

(*Received* 2 *October* 2000 *and in final form* 26 *February* 2001)

As demonstrated in the authors' previous work, damping matrices in the equation of motion of a dynamics system can be identified from the frequency response function matrix (FRM) of the system. A newly developed method with a much simpler algorithm is proposed in this paper for more effective damping matrices identification. Theoretical validation of the method and related noise study are conducted using a simple example, which reveals the method's improved features. A set of specially designed measurements are conducted for a qualitative, experimental validation of the identification method. Important measurement issues learned from the experiment, which include needs for phase matching and FRM conditioning, are explained. Possible significant applications of the method are also discussed.



## 1. INTRODUCTION

A viscous or structural damping model describes the energy loss mechanism in a vibrating system in a simple mathematical form [1]. The modal damping or proportional damping concept further uses an assumption that the spatial distribution of damping follows the mode shape (modal damping) or the system geometry (proportional damping). Such assumptions are obviously not always valid. For example, when a cantilever is assembled to its base structure, a relatively large energy loss mechanism will exist along the interface. If the damping distribution of such a structure is known in more detail, a more accurate stress analysis of the structure will be possible, which will benefit a high cycle fatigue (HCF) analysis of the structure (e.g., a turbine blade). In a high-speed rotor system, different damping mechanisms have different effects on the system stability [2–4]. Therefore, finding different damping mechanisms in respective matrices will improve the quality of the simulation model of such a system.

In most past works, the damping matrix of a structure has been identified using FRFs indirectly. Typically, modal parameters such as natural frequencies and modes are extracted first, then the mass, stiffness and damping matrices using those identified parameters [5–11]. Since damping matrices have a much smaller effect on the system responses compared to the mass and stiffness matrices, the damping matrices identified in this manner become inaccurate. In a typical experimental modal analysis [10, 11], detailed information of the damping effect is usually not a main concern.

Over the past decade, extensive research activities have taken place in model updating, in which the damping matrix is identified as a part of the result. For example, an incremental

0022-460X/01/380505 + 20 $35.00/0 

least-squares method was used for the model updating by Dalenbring [12] and Lee *et al.* [13]. The basic idea of model updating techniques is finding a theoretical model whose response matches best with the measured system response. The damping matrices are identified to match the system response of the experimental and theoretical models, but their uniqueness is not guaranteed.

Tsuei *et al.* [14–16] developed a method that works directly on FRFs to find the damping matrices as the primary objectives of identification. In the authors' previous work [17], a theoretical validation of the method and related noise study were conducted. The authors also attempted an experimental validation of the technique [18], which was incomplete because some necessary measurement techniques were not known at the time.

While the authors were working to conduct an experimental validation of the method proposed by Tsuei, it was realized that a much simpler algorithm could be used.

The method uses a dynamic stiffness matrix (DSM), or the inverse of FRM. The method is very simple, requiring far fewer steps of numerical operations compared to the previously used method. Owing to this simplicity, the identification result is much less influenced by the measurement errors and noises. A theoretical example is used to validate the algorithm and demonstrate advantages of the new method over the previously used method. A set of experimental measurements is devised and conducted to validate the practicality of the method.

## 2. IDENTIFICATION THEORY

### 2.1. DEVELOPMENT OF THE THEORY

The equation of motion of an $n$-degree-of-freedom (d.o.f.) dynamic system subjected to a harmonic input force is

$$M\ddot{x} + C\dot{x} + (\mathrm{j}D + K)x = Fe^{\mathrm{j}\omega t}, \tag{1}$$

where $M$, $C$, $D$ and $K$ are the mass, viscous damping, structural damping and stiffness matrices, respectively, $\mathrm{j} = \sqrt{-1}$, and $x(t)$ and $f(t)$ are the displacement and force vectors. Letting $x(t) = X(\omega)\mathrm{e}^{\mathrm{j}\omega t}$, equation (1) becomes

$$[(K - M\omega^2) + \mathrm{j}(\omega C + D)]\,X(\omega) = F(\omega). \tag{2}$$

The dynamic stiffness matrix (DSM) is defined as

$$[H(\omega)^C]^{-1} = (K - M\omega^2) + \mathrm{j}(\omega C + D), \tag{3}$$

where $H^C(\omega)$ is the frequency response matrix (FRM) defined as

$$H^C(\omega) = [H_{ij}^C] = [X_i/F_j], \quad i, j = 1, 2, 3, \ldots. \tag{4}$$

In equation (4), the superscript $C$ indicates that the variable is a complex quantity, and $H_{ij}^C$ is the frequency response function (FRF) measured between the nodes $i$ and $j$. Because the FRM is much easier to measure than the DSM, the DSM is obtained by inverting the measured FRM.

If the DSM is available, equation (3) can be rewritten as

$$\mathrm{imag}\,(H^C(\omega)^{-1}) = \omega C + D, \qquad \mathrm{real}\,(H^C(\omega)^{-1}) = K - \omega^2 M, \tag{5, 6}$$

where imag and real stand for the imaginary and real parts respectively. For example, $\text{imag}(H^C(\omega)^{-1})$ is the matrix composed of the imaginary part of the DSM matrix $H^C(\omega)^{-1}$. Equations (5) and (6) can be put into

$$[I \quad \omega]\begin{bmatrix} D \\ C \end{bmatrix} = \text{imag}(H^C(\omega)^{-1}), \tag{7}$$

where $I$ is an $n \times n$ identity matrix, and

$$[I \quad -\omega^2]\begin{bmatrix} K \\ M \end{bmatrix} = \text{real}(H^C(\omega)^{-1}). \tag{8}$$

Therefore, the system damping matrices $C$ and $D$ can be found by a pseudo-inverse procedure of equation (7) as

$$\begin{bmatrix} D \\ C \end{bmatrix}_{2n\times n} = \begin{bmatrix} I & \omega_1 I \\ I & \omega_2 I \\ \cdot & \cdot \\ \cdot & \cdot \\ I & \omega_k I \end{bmatrix}^{+}_{kn\times 2n} \begin{bmatrix} \text{imag}(H^C(\omega_1)^{-1}) \\ \text{imag}(H^C(\omega_2)^{-1}) \\ \cdot \\ \cdot \\ \text{imag}(H^C(\omega_k)^{-1}) \end{bmatrix}_{kn\times n}, \tag{9}$$

where $+$ means the pseudo-inverse of the matrix. If necessary, the stiffness and mass matrices can also be found:

$$\begin{bmatrix} K \\ M \end{bmatrix}_{2n\times n} = \begin{bmatrix} I & -\omega_1^2 I \\ I & -\omega_2^2 I \\ \cdot & \cdot \\ \cdot & \cdot \\ I & -\omega_k^2 I \end{bmatrix}^{+}_{kn\times 2n} \begin{bmatrix} \text{real}(H^C(\omega_1)^{-1}) \\ \text{real}(H^C(\omega_2)^{-1}) \\ \cdot \\ \cdot \\ \text{real}(H^C(\omega_k)^{-1}) \end{bmatrix}_{kn\times n}. \tag{10}$$

Equations (9) and (10) have to be set up at least at two frequencies ($k = 2$) to make the equations solvable. Usually, the equations are over-determined by using more frequencies than needed.

As was shown, the procedure itself is surprisingly simple, looking almost like an obvious identity. However, the authors could not find any previous works that used this relationship to find damping matrices. The procedure proposed by Tsuei *et al.* [14–16], which also finds the damping matrices from measured FRFs, may be compared to the proposed method. In the method, $C$ and $D$ matrices are found by solving the following equation:

$$[\omega H^N(\omega) H^N(\omega)]\begin{bmatrix} C \\ D \end{bmatrix} = G(\omega), \tag{11}$$

where $H^N(\omega)$ is the normal FRF, which is defined as

$$H^N(\omega) = [K - M\omega^2]^{-1}. \tag{12}$$

The normal FRF is obtained as

$$H^N(\omega) = H_R^C(\omega) + H_I^C(\omega) H_R^C(\omega)^{-1} H_I^C(\omega), \tag{13}$$

where subscripts $I$ and $R$ stand for the imaginary and real parts, respectively, and $H_R^C(\omega)^{-1}$ is the inverse of the real part of the FRM, i.e. $(\text{real}(H^C))^{-1}$.

$G(\omega)$ is defined as

$$G(\omega) = H_I^C(\omega) H_R^C(\omega)^{-1}. \tag{14}$$

The above method is obviously more involved. The objectives of the identification, elements of the damping matrices, have physically a small effect on the FRM, therefore each of these extra steps amplifies the effect of measurement errors or noises.

If only the viscous damping is used in the modelling, an equivalent viscous damping matrix $C_{eq}$, that represents the entire energy loss mechanism system, can be obtained by solving

$$[C_{eq}]_{n\times n} = \begin{bmatrix} \omega_1 I \\ \omega_2 I \\ \cdot \\ \cdot \\ \omega_k I \end{bmatrix}_{kn\times n}^{+} \begin{bmatrix} \text{imag}(H^C(\omega_1)^{-1}) \\ \text{imag}(H^C(\omega_2)^{-1}) \\ \cdot \\ \cdot \\ \text{imag}(H^C(\omega_k)^{-1}) \end{bmatrix}_{kn\times n}. \tag{15}$$

If only the structural damping is used in the model, an equivalent structural damping matrix $D_{eq}$ can be obtained by solving

$$[D_{eq}]_{n\times n} = \begin{bmatrix} I \\ I \\ \cdot \\ \cdot \\ I \end{bmatrix}_{kn\times n}^{+} \begin{bmatrix} \text{imag}(H^C(\omega_1)^{-1}) \\ \text{imag}(H^C(\omega_2)^{-1}) \\ \cdot \\ \cdot \\ \text{imag}(H^C(\omega_k)^{-1}) \end{bmatrix}_{kn\times n}. \tag{16}$$

### 2.2. THEORETICAL VALIDATION OF THE IDENTIFICATION PROCEDURE

In the author's previous work, a 3-d.o.f. system shown in Figure 1 was used to validate Tsuei's method and to study the noise effect on the identification results [17]. In the validation, 9 FRFs were obtained by solving the matrix equation of motion of the system, which form the FRM. Assuming that this FRM contained the only known measurement data, damping matrices were obtained by the procedure proposed by Tsuei. These matrices were shown to be equal to the damping matrices of the equation of motion. The new algorithm easily passes this test, which validates the identification algorithm itself.

The effect of the measurement noise on the accuracy of the identification was also studied by the authors [17], in which the identification procedure was applied after mixing various levels of random noises to the FRFs. A part of the study is repeated here to compare the proposed method with Tsuei's method. Table 1 compares the identified results from the two methods when 0·5% random noises are mixed in the FRFs for two cases, when the FRM is conditioned and not conditioned. Conditioning FRM involves making the matrix symmetric, to utilize the fact that the FRM is theoretically symmetric. Section 3.2.5 can be referred to for the effect of this conditioning. The comparison shows that the result from the new method is much less sensitive to the measurement noise, giving much better identification results. If the FRM is conditioned, the new method identifies the matrices in

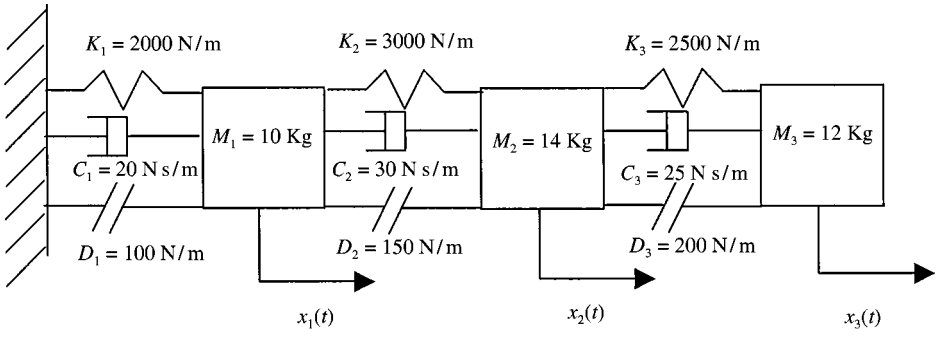


Figure 1. Three d.o.f. lumped parameter model.

TABLE 1

*Comparison of the identification methods: effect of noise on the identified matrices*

| Estimation of damping matrices From the simulation data with 0·5% noise | | | | | | |
|---|---|---|---|---|---|---|
| Estimation method | Viscous damping [$C$] | | | Structural damping [$D$] | | |
| Theoretical matrix | 50 | − 30 | 0 | 250 | − 150 | 0 |
| | − 30 | 55 | − 25 | − 150 | 350 | − 200 |
| | 0 | − 25 | 25 | 0 | − 200 | 200 |
| Tsuei's method | 38·8 | − 19·1 | − 6·4 | 544·5 | − 431·4 | 148·3 |
| (unconditioned) | − 15·7 | 39·4 | − 17·4 | − 608·3 | 816·9 | − 431·0 |
| | − 13·2 | − 10·9 | 17·8 | 263·3 | − 475·0 | 337·3 |
| New method | 49·6 | − 29·3 | 1·3 | 254·0 | − 158·8 | − 21·3 |
| (unconditioned) | − 30·6 | 52·3 | − 21·2 | − 141·9 | 387·3 | − 260·7 |
| | − 0·1 | − 26·8 | 22·4 | 4·5 | − 175·9 | 239·1 |
| Tsuei's method | 45·0 | − 21·9 | − 1·1 | 374·5 | − 361·6 | 19·6 |
| (conditioned) | − 23·7 | 42·5 | − 23·9 | − 361·7 | 716·0 | − 248·3 |
| | − 6·3 | − 13·9 | 23·5 | 129·7 | − 418·8 | 236·3 |
| New method | 49·7 | − 30·0 | 0·6 | 253·4 | − 150·5 | − 9·2 |
| (conditioned) | − 30·0 | 52·6 | − 24·0 | − 150·5 | 381·6 | − 218·5 |
| | 0·6 | − 24·0 | 22·8 | − 9·2 | − 218·5 | 232·6 |

symmetric forms, however the other method does not, which indicates that extra steps in the latter deteriorate the accuracy.

## 3. EXPERIMENTAL VALIDATION OF IDENTIFICATION THEORY

The fact that an experimental identification method is working in a theoretical problem is meaningless unless it also works in real experimental cases. An experimental validation will be necessary to prove the practicality of the method. However, the difficulty in this case was finding a dynamic system whose exact (or theoretical) damping matrices are known. If such a system existed, the validation can be done in a much similar way as the theoretical

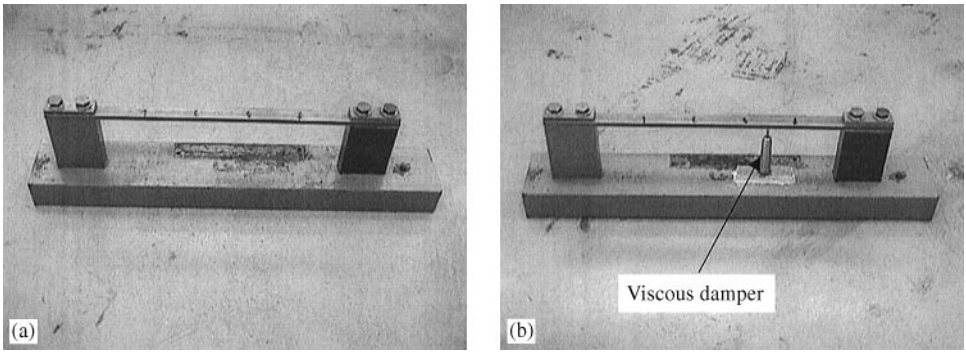


Figure 2. Experimental set-up: (a) clamped beam without a damper, (b) clamped beam with a damper.

validation discussed in the previous section, comparing experimentally identified damping matrices with the theoretical matrices. Not knowing such a system, an indirect, partial validation of the identification method was devised.

Figure 2 shows two systems used in this experiment, a beam configured in two different ways. The system shown in Figure 2(a) is a uniform width beam whose ends are clamped. The system in Figure 2(b) is obtained by attaching a viscous damper to the beam shown in Figure 2(a). Four nodal points are used to define the system as shown in Figure 3, which means that the damping matrices will be identified as $4 \times 4$ matrices. The viscous damper in the latter system was attached between the nodes 3 and 4 as shown in the figure. Accelerations are measured at four nodal points, which are integrated twice to formulate the FRFs in terms of compliances. The multi-reference-impact-testing (MRIT) scheme [19] was used to obtain the FRFs. Roving the excitation to each nodal point, 16 FRFs are obtained, which comprise a $4 \times 4$ FRM. The FRM is inverted to obtain the DSM.

### 3.1. STRATEGY FOR EXPERIMENTAL VALIDATION

The validation strategy is, essentially, to observe whether the identified damping matrices properly reflect the underlying physics and the configurations of the two models, especially if the following facts are observed. (a) The diagonal elements of the damping matrices are positive. (2) The system with the damper (Figure 2(b) shows larger damping matrices, especially the viscous damping matrix, than the system without a damper. (3) The elements of the damping matrices of the system with a damper corresponding to nodes 3 and 4 are relatively large.

Satisfying the above conditions is only a partial validation of the identification theory by itself. However, because the identification algorithm itself was validated theoretically, this partial validation is considered enough from a practical standpoint.

Besides the above three conditions, one may be tempted to use the symmetry of the damping matrices as another observation point. Damping matrices will be identified in symmetric forms if the FRM is symmetric. The FRM, which is theoretically a symmetric matrix, is measured as being slightly non-symmetric. This deviation from the symmetry can be considered the reflection of the quality of the measurement. Therefore, the symmetry of the damping matrices may be useful to evaluate the quality of the measurement but not the quality of the identification. Even for that purpose, using the FRM will be a better option. The FRM may be conditioned to a symmetric form, which seems to improve the identification result significantly as will be explained in section 3.2.5.

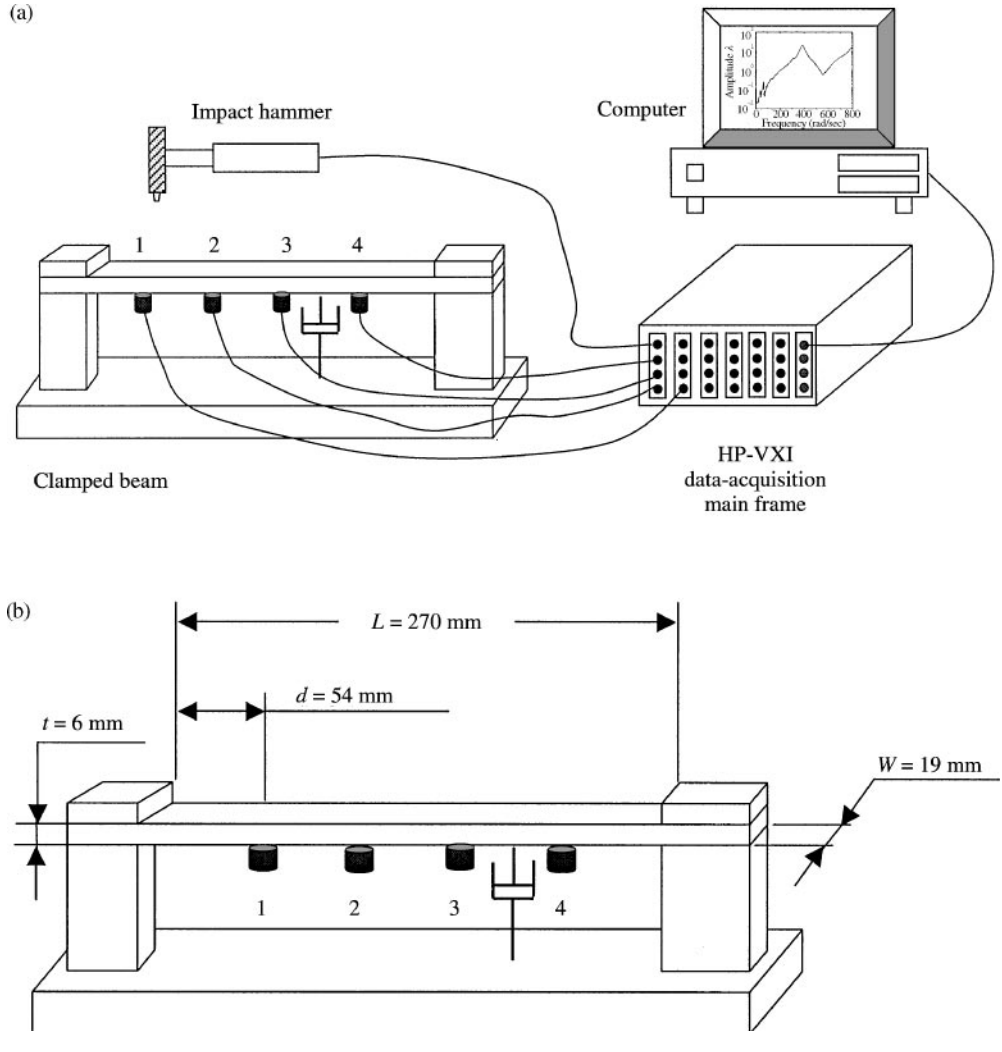


Figure 3. Test set-up: (a) schematic diagram, (b) geometry.

### 3.2. NECESSARY MEASUREMENT AND SIGNAL PROCESSING ISSUES

Several measurement and signal processing issues, some of which are not important in a conventional modal analysis, were realized to be critical in damping matrices identification after many trials and errors during the experiment. These technical issues will be explained one by one.

#### 3.2.1. *D.o.f.s of the experimental model*

The dimension of damping matrices to be identified is determined by the d.o.f.s of the experimental model. For example, if FRFs are measured at four nodes as shown in Figure 3, the matrices are identified as $4 \times 4$ matrices. Using more d.o.f.s would provide better spatial resolution of the damping information, however, at the cost of increased experimental effort. Also, more parameters (elements of damping matrices) to be found will require higher

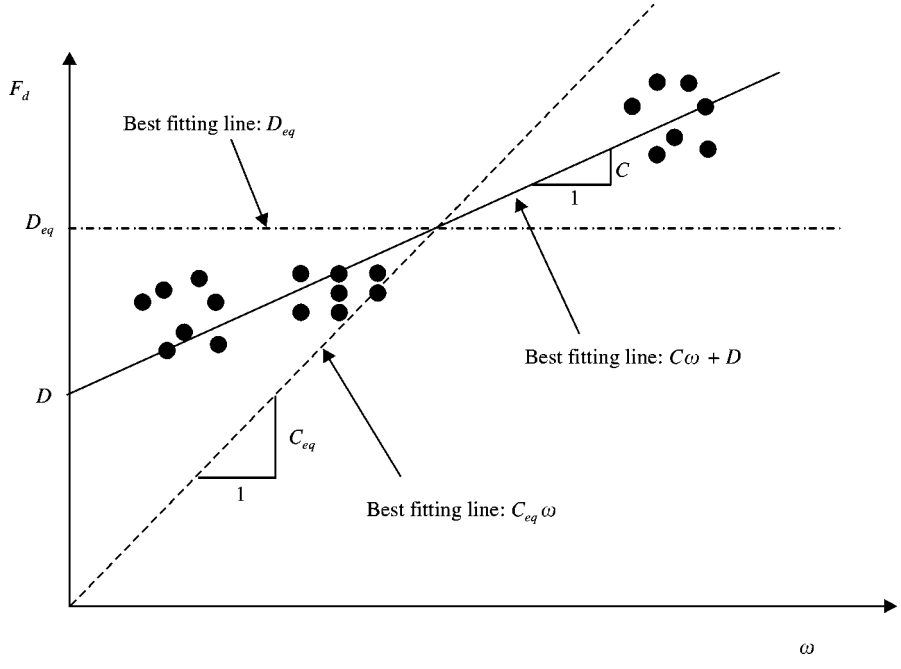


Figure 4. Implication of identifying damping in the viscous and structural damping matrices.

accuracy in the measurement. d.o.f.s of the experimental model will have to be determined considering the necessary spatial resolution and practical limitations.

### 3.2.2. *Selection of frequency range*

Modelling the system equation using $C$ and $D$ matrices implies that the damping force is modelled as a linear function of frequency. As Figure 4 illustrates, the identification process can be considered as trying to find a best fitting straight line from scattered experimental data points representing the damping force. From the figure, it is easy to see that the matrix $D$ will be found more accurately if the FRM data are taken from the low-frequency range to form the identification equation (equation (9)). However, accelerometers generally have poor accuracy in the low-frequency range, which is further deteriorated when integrating acceleration to displacement. Figure 5 is one of the measured FRFs, which shows that the data below 50 Hz are not accurate.

The damping effect on the system response is more pronounced around the resonance frequency (about 383 Hz in this case as seen in Figure 5). Therefore, the measured data have effectively higher signal-to-noise ratios around the resonance frequency. This is why side bands (frequency ranges between half power points) have been used in damping identifications. Considering these facts, the frequency range was chosen as follows in this work. (1) Data below 50 Hz are discarded. (2) The low-frequency range is defined as 50–200 Hz. Using data from this range is expected to provide a more accurate $D$ matrix. (3) The side band was observed as 378–389 Hz for the undamped beam and 374–421 Hz for the damped beam. As a compromise (and also needing over-determination of the identification equation), the side band in this experiment is defined as the range 350–440 Hz. The use of this band is expected to provide a more accurate $C$ matrix.

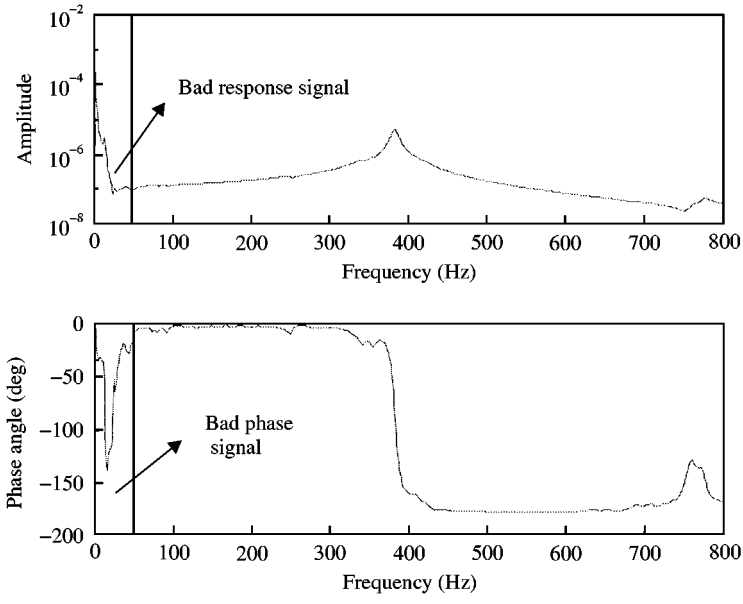


Figure 5. A typical FRF in Bode plot.

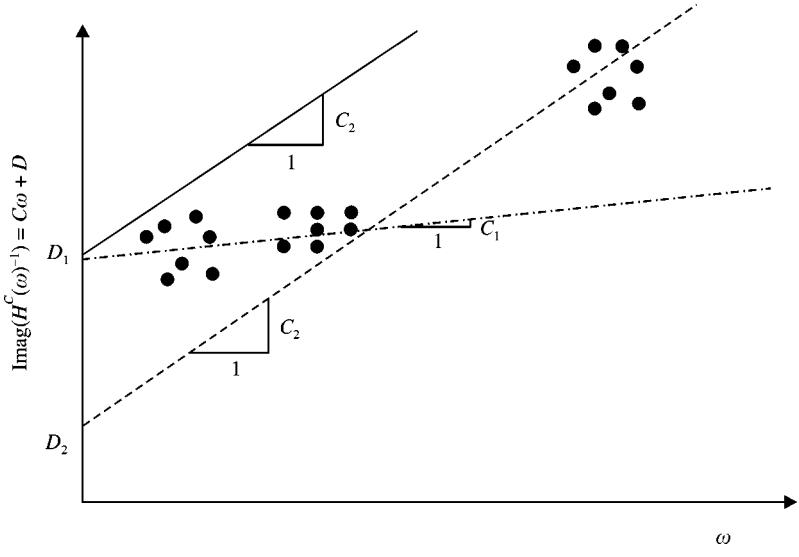


Figure 6. Illustration to explain the mistake to combine $C$ and $D$ matrices identified using different bands: –·–·–·–, identified using low band; – – – –, identified using side band; ——, combined model.

Using the frequency range of interest of the particular problem may also be an option, especially in practical situations.

One may be tempted to combine the $C$ matrix identified by using the side band and the $D$ matrix identified using the low frequency band. Figure 6 illustrates the problem in this approach, which will overestimate or underestimate the damping force.

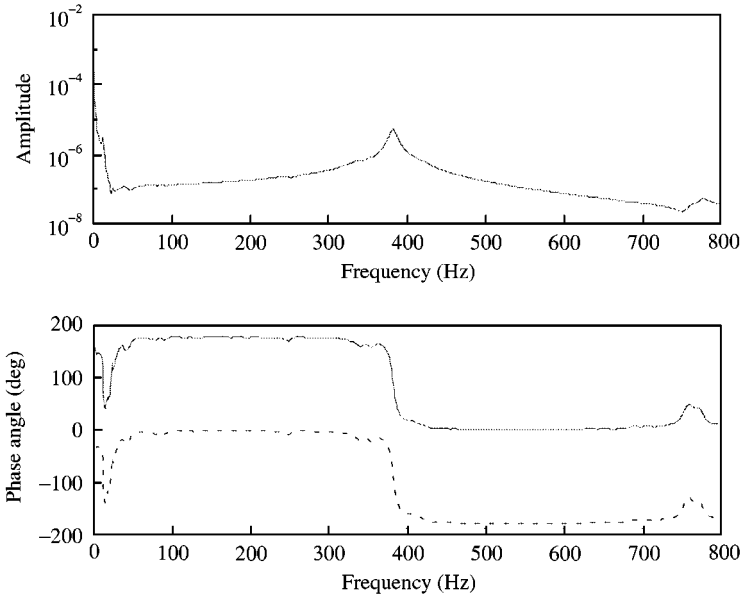


Figure 7. Phase correction of FRF: ——, before correction; – – – –, after correction.

### 3.2.3. *Sign convention of FRFs*

The sign convention of FRFs is not important in a typical modal analysis as long as it is used consistently. In other words, consistent use of either $-X/F$ or $X/F$ would not cause any problem in finding natural frequencies and mode shapes. However, in the identification procedure explained in section 2.1, using $-X/F$ will reverse the sign of the matrices to be identified. Especially, mixed use of sign conventions will make the identification result invalid. The problem can be avoided by making the acceleration and excitation directions the same at all measurement points. For a point where this is not possible, the phase angle of the corresponding FRF has to be corrected numerically. In practice, it will be prudent to check all FRFs and make sure that they all start with zero phase angle at the low-frequency range by adding or subtracting 180° if necessary. Figure 7 shows such a correction that we made for one of the measured FRFs.

### 3.2.4. *Phase matching between the force and motion transducers*

Because the identification uses the imaginary part of the DSM, the FRFs have to be obtained with accurate phase angle, which requires an accurate phase matching between the force and motion transducers. Initially the importance of the phase matching was not realized because it seldom becomes an important issue in conventional modal testing. This problem can be best explained by a single d.o.f. example shown in Figure 8. The FRF of the system is

$$H(\omega) = \frac{X}{F} = \frac{(K - \omega^2 M) - \mathrm{j}(\omega C + D)}{(K - \omega^2 M)^2 + (\omega C + D)^2}. \tag{17}$$

Figure 9 shows the *Argand* plot [1] of this FRF. As the frequency increases, the plot starts from $1/K$ in the real axis and crosses the imaginary axis at point **P**, whose co-ordinate, $-1/(\omega C + D)$, is used to find the equivalent viscous damping $C_{eq} = \omega C + D$.

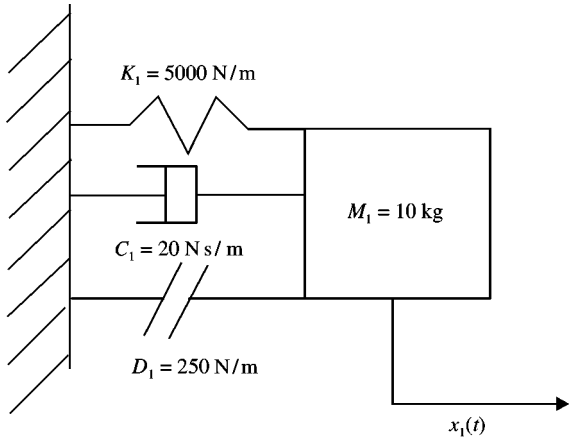


Figure 8. Single d.o.f. system.

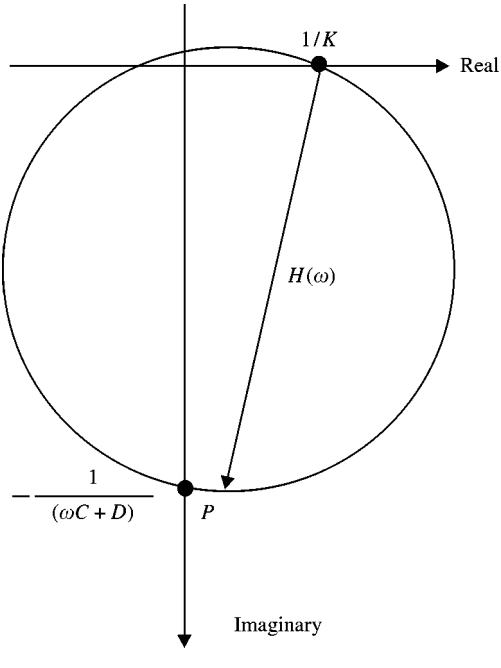


Figure 9. Illustration of damping identification using the *Argand* plot.

Now, suppose that there is a phase angle error of $\phi$ radian between the force and displacement signals. The FRF will be measured as

$$H(\omega) = \frac{(K - \omega^2 M) - \mathrm{j}(\omega C + D)}{(K - \omega^2 M)^2 + (\omega C + D)^2}\, \mathrm{e}^{\mathrm{j}\phi}$$

$$\cong \frac{(K - \omega^2 M) + \phi(\omega C + D) + \mathrm{j}[(K - \omega^2 M)\phi - (\omega C + D)]}{(K - \omega^2 M)^2 + (\omega C + D)^2}. \tag{18}$$

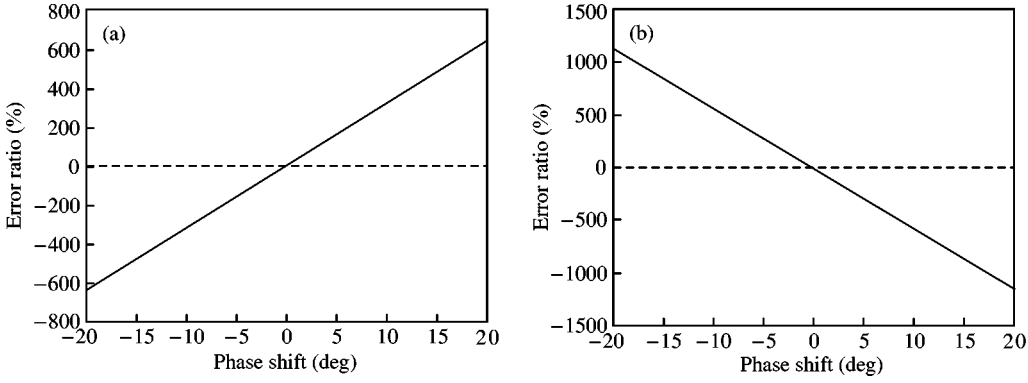


Figure 10. Errors in identified damping as a function of the phase error; – – – –, exact value; ——, identified value: (a) viscous damping $C$; (b) structural damping $D$.

The *Argand* curve crosses the imaginary axis when the real part becomes zero, therefore

$$K - \omega^2 M = -\phi(\omega C + D). \tag{19}$$

By substituting this into equation (18), it is realized that the co-ordinate of this point remains the same because

$$H(\omega) = \frac{-(1+\phi^2)(\omega C + D)}{(1+\phi^2)(\omega C + D)^2} = -\frac{1}{(\omega C + D)}. \tag{20}$$

Therefore, it is seen that the phase mismatch would not affect the damping parameter in this method.

To see the effect of the phase mismatch on the damping matrices identified by the proposed method, let the parameters $M$, $K$, $C$ and $D$ of the system in Figure 8 be 10 Kg, 5000 N/m, 20 N s/m and 250 N/m respectively. Then the proposed method (equation (9)) is applied to find $C$, $D$, $M$ and $K$ for various phase mismatches ($\phi$ rad). Figure 10(a) and (b) shows the errors in the identified $C$ and $D$ matrices as functions of the phase angle error in percentage, i.e., error/exact value $\times$ 100. Figure 11(a–c) represents the errors in the identified $M$, $K$, and the natural frequency. As is shown, the phase mismatch causes much larger errors in $C$ and $D$ compared to other modal parameters.

Figure 12 shows the phase angle between the signals from the force transducer and one of the accelerometers using the ratio calibration set-up [19]. The phase mismatch in Figure 12 is compensated numerically at each frequency to correct 4 FRFs obtained from this set of accelerometers and force transducers. All 16 FRFs are reconstructed in this way before they are used to identify the damping matrices.

### 3.2.5. *Conditioning of the FRM*

An FRM (or DSM) is always measured as slightly non-symmetric, while it is theoretically symmetric. The FRM can be made symmetric by averaging two FRFs, using $(H_{ij} + H_{ji})/2$ for both $H_{ij}$ and $H_{ji}$. It was found that this conditioning not only makes the identified matrices symmetric but also improves the quality of the identification results, perhaps because of the averaging effect. Interestingly, this conditioning did not work well with Tsuei's method. The method identifies non-symmetric damping matrices despite using

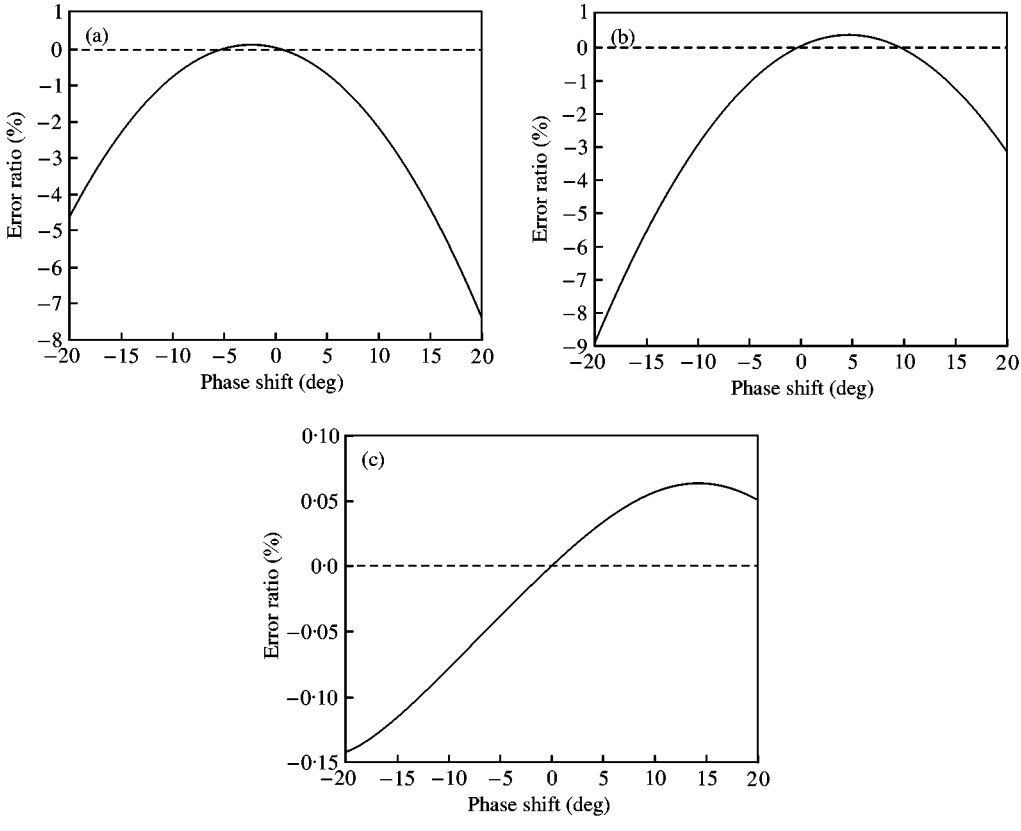


Figure 11. Errors in other identified structural parameters as a function of the phase error: – – – –, exact value; ——, identified value; (a) mass $M$, (b) stiffness $K$, (c) natural frequency $\omega_n$.

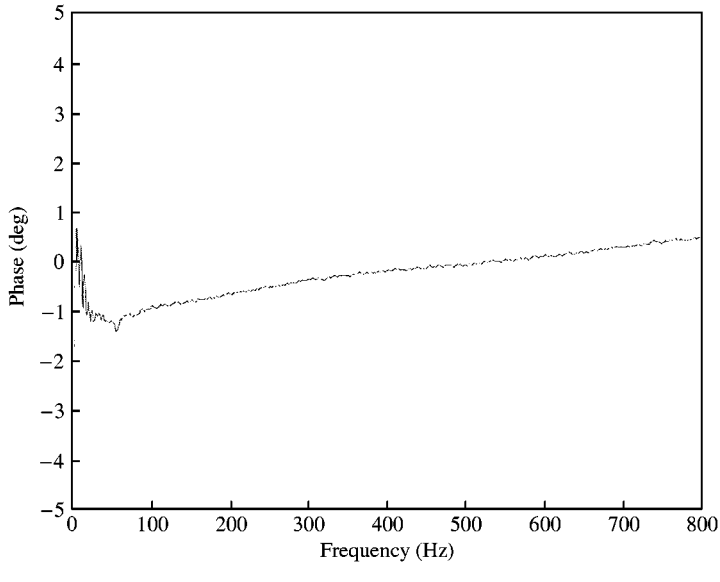


Figure 12. Phase mismatch found from the calibration.

TABLE 2

*Summary of experimental comparisons*

| Table No. | Frequency range (Hz) | Phase match | FRM conditioning |
|---|---|---|---|
| (a) *Summary of Tables* 3–9 | | | |
| 3 | 350–440 (side band) | No | No |
| 4 | 350–440 (side band) | Yes | No |
| 5 | 350–440 (side band) | Yes | Yes |
| 6 | 50–200 (low band) | Yes | Yes |
| 7 | 50–120 (low band) | Yes | Yes |
| 8 | 300–480 | Yes | Yes |
| 9 | 50–800 | Yes | Yes |

(b) *Purposes of comparisons*

| Comparison | Effect to discuss |
|---|---|
| Table 3 versus Table 4 | Phase matching |
| Table 4 versus Table 5 | FRM conditioning |
| Table 5 versus Table 6 | Low frequency versus side band |
| Table 6 versus Table 7, Table 5 versus Table 8 | General frequency dependence |
| Table 9 versus Table 5, Table 9 versus Table 6 | Wide range versus low range versus high range |

a conditioned FRM, which may have been caused by the accumulation of numerical errors due to the extra steps of the method.

## 4. EXPERIMENTAL RESULTS

Table 2 summarizes all the subsequent tables, how they were obtained and compared to one another. For example, the table shows that the damping matrices in Table 3 were identified using the FRM neither phase matched nor conditioned and using the side band (350 and 440 Hz). Table 2(b) summarizes the purposes of the comparisons made. All tables show the damping matrices in the same format, listing $C$, $D$, $C_{eq}$ and $D_{eq}$ matrices for two systems. Generally, the different configurations of the two systems are reflected reasonably well in all cases. For example, damping matrices of the system with a damper have larger damping matrices in all tables.

The effect of the phase matching can be seen by comparing Tables 3 and 4, and the effect of the FRM conditioning can be seen by comparing Tables 4 and 5. Phase matching improves the result in general, especially judging from the equivalent matrices identified, whose diagonal elements become nearly all positive in Table 4 as the phase is matched. Comparing Tables 4 and 5 shows that the effect of the FRM conditioning improves the identification results in an overall sense from the three observation points of view described in section 3.1. It is believed that the averaging effect of the FRM conditioning improves the result in addition to the obvious effect of making the matrices symmetric.

By comparing Tables 5 and 6, it can be seen that the structural damping matrix obtained is of higher quality if the lower frequency band data are used. Substantially different matrices are obtained depending on whether the side band or the low band is used. This indicates that the actual damping mechanism of the system is not a linear function but a higher order

TABLE 3

*Damping matrices identified using side band* (350–440 *Hz*), *neither phase matched nor FRM conditioned*

| Beam without a damper | | | | | Beam with a damper | | |
|---|---|---|---|---|---|---|---|
| | | | $[C]$ ($\times 10^3$ N s/m) | | | | |
| 1·1318 | − 1·6250 | 0·8173 | 0·6457 | − 0·8416 | − 0·6190 | 1·5215 | 1·8753 |
| − 0·5126 | 0·6619 | − 0·5434 | 0·7226 | − 0·1760 | 1·1703 | − 2·8448 | 0·5616 |
| − 0·0070 | 0·3994 | − 0·2157 | − 1·0081 | 1·4290 | − 1·2683 | 2·5515 | − 3·9828 |
| 0·2272 | − 1·2311 | 1·2964 | − 0·2292 | − 1·2553 | 0·3481 | − 1·7293 | 4·7676 |
| | | | $[D]$ ($\times 10^7$ N/m) | | | | |
| − 0·1858 | 0·4982 | − 0·4772 | 0·2173 | 0·4681 | 0·0902 | − 0·4990 | − 0·7435 |
| 0·2111 | − 0·2418 | 0·1912 | − 0·1926 | 0·0600 | − 0·4265 | 0·9336 | 0·2835 |
| − 0·1659 | − 0·0894 | 0·2885 | − 0·3181 | − 0·5578 | 0·5076 | − 0·7204 | 0·3502 |
| 0·1436 | 0·3649 | − 0·7875 | 1·1489 | 0·5668 | − 0·2258 | 0·4032 | − 0·2739 |
| | | | $[C]_{eq}$ ($\times 10^3$ N s/m) | | | | |
| 0·5911 | − 0·1749 | − 0·5715 | 1·2781 | 0·4078 | − 0·3781 | 0·1897 | − 0·1092 |
| 0·1017 | − 0·0419 | 0·0131 | 0·1620 | − 0·0157 | 0·0319 | − 0·3530 | 1·3183 |
| − 0·4898 | 0·1393 | 0·6240 | − 1·9338 | − 0·0598 | 0·0865 | 0·6288 | − 3·0479 |
| 0·6450 | − 0·1690 | − 0·9954 | 3·1146 | 0·2576 | − 0·2546 | − 0·6531 | 4·0364 |
| | | | $[D]_{eq}$ ($\times 10^7$ N/m) | | | | |
| 0·1876 | − 0·0378 | − 0·2076 | 0·4303 | 0·1674 | − 0·1295 | 0·0411 | − 0·0778 |
| 0·0420 | − 0·0235 | 0·0119 | 0·0458 | − 0·0024 | − 0·0111 | − 0·0763 | 0·4829 |
| − 0·1682 | 0·0424 | 0·2174 | − 0·6506 | − 0·0506 | 0·0574 | 0·1854 | − 1·0636 |
| 0·2185 | − 0·0412 | − 0·3598 | 1·0733 | 0·1212 | − 0·1022 | − 0·2107 | 1·4185 |

TABLE 4

*Damping matrices identified using side band* (350–440 *Hz*), *phase matched but not FRM conditioned*

| Beam without a damper | | | | | Beam with a damper | | |
|---|---|---|---|---|---|---|---|
| | | | $[C]$ ($\times 10^3$ N s/m) | | | | |
| 1·2635 | − 1·7413 | 0·8112 | 0·6855 | − 0·5608 | − 0·9803 | 1·6949 | 1·7637 |
| − 0·5573 | 0·7724 | − 0·6528 | 0·8460 | − 0·3672 | 1·5027 | − 3·1251 | 0·8403 |
| − 0·0603 | 0·3219 | − 0·0627 | − 1·3295 | 1·4531 | − 1·4925 | 2·8084 | − 4·4144 |
| 0·2751 | − 1·2152 | 1·1389 | 0·1514 | − 1·2022 | 0·3792 | − 1·9071 | 5·1599 |
| | | | $[D]$ ($\times 10^7$ N/m) | | | | |
| − 0·2276 | 0·5288 | − 0·4740 | 0·2080 | 0·3758 | − 0·4588 | 0·2367 | − 0·1534 |
| 0·2235 | − 0·2707 | 0·2198 | − 0·2235 | − 0·0413 | 0·1057 | − 0·4282 | 1·4173 |
| − 0·1476 | − 0·0690 | 0·2471 | − 0·2400 | − 0·0574 | 0·0347 | 0·6983 | − 3·2005 |
| 0·1278 | 0·3609 | − 0·7443 | 1·0581 | 0·2656 | − 0·2455 | − 0·7016 | 4·1811 |
| | | | $[C]_{eq}$ ($\times 10^3$ N s/m) | | | | |
| 0·6012 | − 0·2023 | − 0·5683 | 1·2909 | 0·4421 | − 0·4588 | 0·2367 | − 0·1534 |
| 0·0930 | − 0·0156 | 0·0132 | 0·1954 | − 0·0413 | 0·1057 | − 0·4282 | 1·4173 |
| − 0·4898 | 0·1209 | 0·6566 | − 2·0278 | − 0·0574 | 0·0347 | 0·6983 | − 3·2005 |
| 0·6472 | − 0·1649 | − 1·0274 | 3·2310 | 0·2656 | − 0·2455 | − 0·7016 | 4·1811 |
| | | | $[D]_{eq}$ ($\times 10^7$ N/m) | | | | |
| 0·1892 | − 0·0456 | − 0·2064 | 0·4341 | 0·1767 | − 0·1526 | 0·0553 | − 0·0922 |
| 0·0396 | − 0·0160 | 0·0044 | 0·0555 | − 0·0082 | 0·0100 | − 0·0989 | 0·5145 |
| − 0·1675 | 0·0371 | 0·2264 | − 0·6785 | − 0·0501 | 0·0424 | 0·2064 | − 1·1123 |
| 0·2186 | − 0·0400 | − 0·3687 | 1·1081 | 0·1232 | − 0·0995 | − 0·2253 | 1·4650 |

TABLE 5

*Damping matrices identified using side band (350–440 Hz), phase matched and FRM conditioned*

| Beam without a damper | | | | | Beam with a damper | | |
|---|---|---|---|---|---|---|---|
| | | | $[C]$ ($\times 10^3$ N s/m) | | | | |
| 4·4470 | − 1·1606 | − 1·2195 | 0·1236 | 3·7244 | − 2·9250 | − 2·1366 | 8·8274 |
| − 1·1606 | 0·8093 | 0·0355 | − 0·8394 | − 2·9250 | 3·6654 | − 0·6137 | − 5·7900 |
| − 1·2195 | 0·0355 | 1·0391 | − 1·1003 | − 2·1366 | − 0·6137 | 2·3144 | − 1·5113 |
| 0·1236 | − 0·8394 | − 1·1003 | 4·6854 | 8·8274 | − 5·7900 | − 1·5113 | 7.0014 |
| | | | $[D]$ ($\times 10^7$ N/m) | | | | |
| − 1·3414 | 0·3753 | 0·1559 | 0·5187 | − 1·1006 | 0·9069 | 0·6684 | − 2·8563 |
| 0·3753 | − 0·2731 | 0·0199 | 0·2401 | 0·9069 | − 1·2101 | 0·1545 | 2·1703 |
| 0·1559 | 0·0199 | − 0·0159 | − 0·3262 | 0·6684 | 0·1545 | − 0·2671 | − 0·5605 |
| 0·5187 | 0·2401 | − 0·3262 | − 0·2728 | − 2·8563 | 2·1703 | − 0·5905 | − 0·2532 |
| | | | $[C]_{eq}$ ($\times 10^3$ N s/m) | | | | |
| 0·5431 | − 0·0684 | − 0·7658 | 1·6333 | 0·7872 | − 0·5047 | − 0·3527 | 1·2044 |
| − 0·0684 | 0·0144 | 0·0934 | − 0·1407 | − 0·5047 | 0·4358 | − 0·2015 | 0·0022 |
| − 0·7658 | 0·0934 | 0·9928 | − 2·0496 | − 0·3527 | − 0·2015 | 1·6015 | − 3·0873 |
| 1·6333 | − 0·1407 | − 2·0496 | 3·8914 | 1·2044 | 0·0022 | − 3·0873 | 6·3257 |
| | | | $[D]_{eq}$ ($\times 10^7$ N/m) | | | | |
| 0·1256 | − 0·0076 | − 0·2464 | 0·5595 | 0·2216 | − 0·1356 | − 0·0901 | 0·2774 |
| − 0·0076 | − 0·0062 | 0·0316 | − 0·0368 | − 0·1315 | 0·0911 | − 0·0634 | 0·1149 |
| − 0·2464 | 0·0316 | 0·3269 | − 0·6891 | − 0·0901 | − 0·0634 | 0·5545 | − 1·1270 |
| 0·5595 | − 0·0368 | − 0·6891 | 1·2727 | 0·2774 | 0·1149 | − 1·1270 | 2·2323 |

TABLE 6

*Damping matrices identified using low band (50–200 Hz), phase matched and FRM conditioned*

| Beam without a damper | | | | | Beam with a damper | | |
|---|---|---|---|---|---|---|---|
| | | | $[C]$ ($\times 10^3$ N s/m) | | | | |
| 0·0145 | − 0·0137 | − 0·0004 | 0·0288 | 0·0020 | 0·0021 | − 0·0045 | 0·0063 |
| − 0·0137 | 0·0160 | − 0·0073 | − 0·0036 | 0·0021 | − 0·0054 | 0·0047 | − 0·0005 |
| − 0·0004 | − 0·0073 | 0·0259 | − 0·0475 | − 0·0045 | 0·0047 | 0·0011 | − 0·0116 |
| 0·0288 | − 0·0036 | − 0·0475 | 0·0999 | 0·0063 | − 0·0005 | − 0·0116 | 0.0276 |
| | | | $[D]$ ($\times 10^7$ N/m) | | | | |
| 0·3286 | − 0·1718 | − 0·0366 | 0·0348 | 0·4302 | − 0·3631 | 0·2830 | − 0·2731 |
| − 0·1718 | 0·2560 | − 0·2221 | 0·0836 | − 0·3631 | 0·4231 | − 0·4152 | 0·3087 |
| − 0·0366 | − 0·2221 | 0·2288 | − 0·1070 | 0·2803 | − 0·4152 | 0·4436 | − 0·3237 |
| 0·0348 | 0·0836 | − 0·1070 | 0·2799 | − 0·2731 | 0·3087 | − 0·3237 | 0·3816 |
| | | | $[C]_{eq}$ ($\times 10^3$ N s/m) | | | | |
| 3·7456 | − 1·9648 | − 0·4160 | 0·4240 | 4·8866 | − 4·1207 | 3·2087 | − 3·0947 |
| − 1·9648 | 2·9224 | − 2·5287 | 0·9461 | − 4·1207 | 4·7976 | − 4·7092 | 3·5047 |
| − 0·4160 | − 2·5287 | 2·6242 | − 1·2622 | 3·2087 | − 4·7092 | 5·0379 | − 3·6867 |
| 0·4240 | 0·9461 | − 1·2622 | 3·2776 | − 3·0947 | 3·5047 | − 3·6867 | 4·3606 |
| | | | $[D]_{eq}$ ($\times 10^7$ N/m) | | | | |
| 0·3298 | − 0·1729 | − 0·0366 | 0·0370 | 0·4304 | − 0·3630 | 0·2827 | − 0·2726 |
| − 0·1729 | 0·2572 | − 0·2226 | 0·0833 | − 0·3630 | 0·4226 | − 0·4148 | 0·3087 |
| − 0·0366 | − 0·2226 | 0·2309 | − 0·1107 | 0·2827 | − 0·4148 | 0·4437 | − 0·3246 |
| 0·0370 | 0·0833 | − 0·1107 | 0·2877 | − 0·2726 | 0·3087 | − 0·3246 | 0·3838 |

TABLE 7

*Damping matrices identified using a different low band* (50–120 *Hz*), *phase matched and FRM conditioned*

| Beam without a damper | | | | | Beam with a damper | | |
|---|---|---|---|---|---|---|---|
| | | | $[C]$ ($\times 10^3$ N s/m) | | | | |
| 0·0160 | − 0·0151 | − 0·0004 | 0·0316 | 0·0020 | 0·0023 | − 0·0050 | 0·0069 |
| − 0·0151 | 0·0176 | − 0·0081 | − 0·0040 | 0·0023 | − 0·0060 | 0·0052 | − 0·0006 |
| − 0·0004 | − 0·0081 | 0·0285 | − 0·0519 | − 0·0050 | 0·0052 | 0·0012 | − 0·0127 |
| 0·0316 | − 0·0040 | − 0·0519 | 0·1091 | 0·0069 | − 0·0006 | − 0·0127 | 0.0303 |
| | | | $[D]$ ($\times 10^7$ N/m) | | | | |
| 0·3285 | − 0·1718 | − 0·0366 | 0·0346 | 0·4302 | − 0·3631 | 0·2830 | − 0·2732 |
| − 0·1718 | 0·2559 | − 0·2220 | 0·0836 | − 0·3631 | 0·4231 | − 0·4152 | 0·3087 |
| − 0·0366 | − 0·2220 | 0·2287 | − 0·1067 | 0·2803 | − 0·4152 | 0·4436 | − 0·3236 |
| 0·0346 | 0·0836 | − 0·1067 | 0·2794 | − 0·2732 | 0·3087 | − 0·3236 | 0·3815 |
| | | | $[C]_{eq}$ ($\times 10^3$ N s/m) | | | | |
| 5·8306 | − 3·0552 | − 0·6483 | 0·6449 | 7·6161 | − 6·4245 | 5·0042 | − 4·8275 |
| − 3·0552 | 4·5465 | − 3·9377 | 1·4769 | − 6·4245 | 7·4816 | − 7·3432 | 5·4635 |
| − 0·6483 | − 3·9377 | 4·0762 | − 1·9411 | 5·0042 | − 7·3432 | 7·8524 | − 5·7404 |
| 0·6449 | 1·4769 | − 1·9411 | 5·0535 | − 4·8275 | 5·4635 | − 5·7404 | 6·7819 |
| | | | $[D]_{eq}$ ($\times 10^7$ N/m) | | | | |
| 0·3294 | − 0·1726 | − 0·0366 | 0·0363 | 0·4303 | − 0·3630 | 0·2828 | − 0·2728 |
| − 0·1726 | 0·2568 | − 0·2225 | 0·0834 | − 0·3630 | 0·4228 | − 0·4150 | 0·3087 |
| − 0·0364 | − 0·2225 | 0·2302 | − 0·1095 | 0·2828 | − 0·4150 | 0·4437 | − 0·3243 |
| 0·0363 | 0·0834 | − 0·1095 | 0·2852 | − 0·2728 | 0·3087 | − 0·3243 | 0·3831 |

function of frequency. For example, the small damper used in the experiment will be neither viscous nor constant. Considering this, one may use the frequency band of interest to identify the damping matrices. If the range is too wide, a piecewise linear model or a non-linear damping model may have to be used. For the latter, the identification method will have to be modified to include higher order terms.

Comparisons of Tables 6 and 7, and Tables 5 and 8 show that a small change in the frequency range results also in small changes in the identified matrices. This indicates that the large differences between the results in Tables 5 (obtained using the side band) and 6 (obtained using the low band) were not caused by a numerical problem but by the nature of the system.

Table 9 shows the identification results obtained using a wide frequency range (50–800 Hz), which includes both the side band and low band. Such a result may be used to represent the system in an average sense for a wide frequency range of interest as an alternative to a piecewise or non-linear model.

Another interesting observation is that while the beam without a damper has a symmetric geometry, the identified result does not reflect the symmetry (e.g., $D_{11}$ is quite different from $D_{44}$ in Table 5). However, the geometric symmetry is better represented in the $C$ matrix when the side band is used (see Table 5), and in the $D$ matrix when the low band is used (see Table 6), which is consistent with the previous discussions. During our experiment, it was observed that even a small distortion of the system results in substantially different damping matrices, which also do not show any geometric symmetry. This may be explained by the fact that a variation of the geometry or clamping conditions, even if they are small, can cause significant changes in the energy loss mechanism. This feature may be exploited for

TABLE 8

*Damping matrices identified using a different side band* (300–480 *Hz*), *phase matched and FRM conditioned*

| Beam without a damper | | | | | Beam with a damper | | |
|---|---|---|---|---|---|---|---|
| | | | $[C]$ ($\times 10^3$ N s/m) | | | | |
| 3·3420 | − 1·0509 | − 0·8668 | 0·3595 | 3·1503 | − 2·3648 | − 2·1231 | 7·6908 |
| − 1·0509 | 0·7685 | − 0·0740 | − 0·5962 | − 2·3648 | 3·1607 | − 0·5468 | − 4·8655 |
| − 0·8668 | − 0·0740 | 0·9520 | − 0·8996 | − 2·1231 | − 0·5468 | 1·7178 | − 0·8123 |
| 0·3595 | − 0·5962 | − 0·8996 | 3·0084 | 7·6908 | − 4·8655 | − 0·8123 | 4.7971 |
| | | | $[D]$ ($\times 10^7$ N/m) | | | | |
| − 0·9383 | 0·3355 | 0·0267 | 0·4332 | − 0·9086 | 0·7243 | 0·6557 | − 2·4704 |
| 0·3355 | − 0·2587 | 0·0601 | 0·1513 | 0·7243 | − 1·0421 | 0·1324 | 1·8607 |
| 0·0267 | 0·0601 | 0·0157 | − 0·3995 | 0·6557 | 0·1324 | − 0·0820 | − 0·7967 |
| 0·4332 | 0·1513 | − 0·3995 | 0·3390 | − 2·4704 | 1·8607 | − 0·7967 | 0·4332 |
| | | | $[C]_{eq}$ ($\times 10^3$ N s/m) | | | | |
| 0·5395 | − 0·0486 | − 0·7869 | 1·6534 | 0·7059 | − 0·4162 | − 0·3593 | 1·0451 |
| − 0·0486 | − 0·0042 | 0·1057 | − 0·1442 | − 0·4162 | 0·3573 | − 0·1905 | 0·1401 |
| − 0·7869 | 0·1057 | 0·9992 | − 2·0930 | − 0·3593 | − 0·1905 | 1·4972 | − 2·9555 |
| 1·6534 | − 0·1442 | − 2·0930 | 4·0211 | 1·0451 | 0·1401 | − 2·9555 | 5·9626 |
| | | | $[D]_{eq}$ ($\times 10^7$ N/m) | | | | |
| 0·1221 | 0·0021 | − 0·2483 | 0·5473 | 0·1998 | − 0·1077 | − 0·0914 | 0·2357 |
| 0·0021 | − 0·0149 | 0·0367 | − 0·0379 | − 0·1077 | 0·0700 | − 0·0599 | 0·1488 |
| − 0·2483 | 0·0367 | 0·3179 | − 0·6850 | − 0·0914 | − 0·0599 | 0·5224 | − 1·0825 |
| 0·5473 | − 0·0379 | − 0·6850 | 1·2936 | 0·2357 | 0·1488 | − 1·0825 | 2·1212 |

TABLE 9

*Damping matrices identified using wide band* (50–800 *Hz*), *phase matched and FRM conditioned*

| Beam without a damper | | | | | Beam with a damper | | |
|---|---|---|---|---|---|---|---|
| | | | $[C]$ ($\times 10^3$ N s/m) | | | | |
| − 4·435 | 4·433 | − 1·313 | − 3·273 | − 3·5075 | 0·2278 | 0·8480 | − 0·5235 |
| 4·433 | − 6·299 | 4·269 | − 0·269 | 0·2278 | 1·6700 | − 0·9352 | − 1·8994 |
| − 1·313 | 4·269 | − 5·396 | 5·293 | 0·8480 | − 0·9352 | − 0·4527 | 4·1053 |
| − 3·273 | − 0·269 | 5·293 | − 10·638 | − 0·5235 | − 1·8994 | 4·1053 | − 8.7964 |
| | | | $[D]$ ($\times 10^7$ N/m) | | | | |
| 1·7203 | − 1·6192 | 0·3256 | 1·5447 | 1·5154 | − 0·2711 | − 0·4127 | 0·6572 |
| − 1·6192 | 2·3095 | − 1·5800 | 0·1207 | − 0·2711 | − 0·3965 | 0·2042 | 0·7000 |
| 0·3256 | − 1·5800 | 2·3361 | − 2·6984 | − 0·4127 | 0·2042 | 0·8626 | − 2·7609 |
| 1·5447 | 0·1207 | − 2·6984 | 5·4880 | 0·6572 | 0·7000 | − 2·7609 | 5·8292 |
| | | | $[C]_{eq}$ ($\times 10^3$ N s/m) | | | | |
| 0·6770 | − 0·3787 | − 0·3454 | 1·3174 | 0·9957 | − 0·5779 | − 0·3783 | 1·4296 |
| − 0·3787 | 0·5641 | − 0·4263 | 0·0898 | − 0·5779 | 0·4916 | − 0·3285 | 0·1808 |
| − 0·3454 | − 0·4263 | 1·5462 | − 2·7253 | − 0·3783 | − 0·3285 | 2·1106 | − 4·0989 |
| 1·3174 | 0·0898 | − 2·7253 | 5·6706 | 1·4296 | 0·1808 | − 4·0989 | 8·5258 |
| | | | $[D]_{eq}$ ($\times 10^7$ N/m) | | | | |
| 0·5360 | − 0·4355 | − 0·0250 | 0·6708 | 0·5788 | − 0·2103 | − 0·1862 | 0·5175 |
| − 0·4355 | 0·6275 | − 0·4401 | 0·0489 | − 0·2103 | 0·0494 | − 0·0456 | 0·1928 |
| − 0·0250 | − 0·4401 | 0·8953 | − 1·2849 | − 0·1862 | − 0·0456 | 0·7417 | − 1·6646 |
| 0·6708 | 0·0489 | − 1·2849 | 2·6474 | 0·5175 | 0·1928 | − 1·6646 | 3·4803 |

a positive purpose. For example, identified damping matrices may be used to inspect the quality of the assembly of high-precision equipment.

## 5. SUMMARY AND CONCLUSION

A new algorithm was proposed for the experimental identification of the damping matrices, which identifies the viscous and structural damping matrices of the equation of motion of a dynamic system. The new algorithm is very simple, and therefore provides more accurate and robust results compared to the method previously used [14]. Theoretical validation of the method and the related noise study were conducted using a 3 d.o.f. lumped parameter system. A set of measurements were taken, which served as a qualitative, experimental validation of the procedure. Important measurement techniques necessary for correct implementation of the proposed method learned from the experiment were also reported, which included phase matching of FRFs, conditioning of the FRM and the selection of the frequency range.

The method identifies damping matrices, which carry a lot more information than damping ratios; therefore it will enable some interesting applications. The following are considered potentially promising applications.

(1) FEA-experiment hybrid modelling of a dynamic system: the mass and stiffness matrices are formulated theoretically, and the damping matrices are identified experimentally, which are then combined to obtain the system model. Because the actual spatial distribution of the damping is considered in the model, this will provide a more accurate analysis.
(2) Identified damping matrices may be used as valuable information for design or inspection. For example, comparison of the spatial distributions of damping of a new design and an existing design may provide good insights to designers. Because even a very small change in the system causes a significant change in identified damping matrices, the matrices may also be used for an inspection purpose.
(3) The method will be very useful if it is extended and applied to modelling of rotor systems. The ability of the method to distinguish different damping mechanisms will be very helpful in rotor systems, because different damping mechanisms have different effects on the system stability.

The accuracy of the identified damping matrices depends almost entirely on the accuracy of the measured FRFs, especially their phase angles. Therefore, the techniques used to measure FRFs will be critical to the feasibility of the above applications.

## ACKNOWLEDGMENTS

The authors acknowledge the financial support of ArvinMeritor Industries related to this work.

## REFERENCES

1. W. T. THOMSON and M. D. DAHLEH 1998 *Theory of Vibration with Applications*. Englewood Cliffs, NJ: Prentice-Hall.
2. S. H. CRANDALL 1995 *Nonlinear Dynamics and Stochastic Mechanics* (W. Kielmann and N. S. Namachivaya, editors), 1–44. Boca Raton: CRC Press. Rotordynamics.

3. C. KESSLER and J. KIM 1998 *Proceedings of the* 16*th International Modal Analysis Conference*, *Santa Barbara*, *CA*, 782–787. Complex modal analysis and interpretation for rotating machinery.
4. C. KESSLER and J. KIM 1999 *Proceedings of the* 17*th International Modal Analysis Conference*, *Orlando*, *FL*, 1930–1937. Complex modal analysis and modal superposition for rotating machinery.
5. D. F. PILKEY and D. J. INMAN 1997 *Proceedings of the* 15*th International Modal Analysis Conference*, *Orlando*, *FL*, 1152–1157. An iterative approach to viscous damping matrix identification.
6. P. LANCASTER 1961 *Journal of the Aerospace Sciences* **28**, 256–256. Expression for damping matrices in linear vibration problems.
7. P. EBERSBACH and H. IRRETIER 1989 *Journal of Analytical and Experimental Modal Analysis* **4**, 109–116. On the application of modal parameter estimation using frequency domain algorithms.
8. R. J. ALLEMANG and D. L. BROWN 1998 *Journal of Sound and Vibration* **211**, 301–322. A unified matrix polynomial approach to modal identification.
9. J. M. LEURIDAN, D. L. BROWN and R. ALLEMANG 1982 *Proceedings of the* 23*rd Structures*, *Structural Dynamics and Materials Conference*, Part 2, AIAA Paper No. 82-0767. Direct system parameter identification of mechanical structures with application to modal analysis.
10. C. W. BERT 1973 *Journal of Sound and Vibration* **29**, 129–153. Material damping: an introductory review of mathematical models, measures and experimental techniques.
11. D. J. EWINS 1986 *Modal Testing*: *Theory and Practice*. Letchworth, Hertfordshire, England: Research Studies Press Ltd. and Brüel & Kjaer.
12. M. DALENBRING 1999 *Mechanical Systems and Signal Processing* **13**, 547–569. Damping function estimation based on measured vibration frequency responses and finite-element displacement Modes.
13. H. G. LEE and B. J. DOBSON 1991 *Journal of Sound and Vibration* **145**, 61–81. The direct measurement of structural mass, stiffness and damping properties.
14. Y. G. TSUEI and B. K. HUANG 1998 *Proceedings of the* 16*th International Modal Analysis Conference*, *Santa Barbara*, *CA*, 1427–1432. Effect of modeling for damping on parameter identification.
15. S. Y. CHEN and Y. G. TSUEI 1997 *Proceeding of the* 15*th International Modal Analysis Conference*, *Orlando*, *FL*, 1139–1144. Effect of parameter identification on modeling of viscous and structural damping.
16. S. Y. CHEN, M. S. JU and Y. G. TSUEI 1996 *American Society of Mechanical Engineers Journal of Vibration and Acoustics* **118**, 78–82. Estimation of mass, stiffness and damping matrices from frequency response functions.
17. J. H. LEE and J. KIM *Journal of Sound and Vibration* **240**, 545–565. Direct identification of damping matrices from measured frequency response functions.
18. J. H. LEE and J. KIM 2000 *Proceedings of International Compressor Conference at Purdue University*, 869–876. Direct identification of damping parameters from FRF and its application to compressor engineering.
19. R. J. ALLEMANG and D. L. BROWN 1995 *Shock and Vibration Handbook* (C.M. Harris and C. E. Crede, editors). New York: McGraw-Hill Book Company; Chapter 21, fourth edition. Experimental modal analysis.